Chemical Science

ROYAL SOCIETY OF CHEMISTRY

EDGE ARTICLE

View Article Online
View Journal | View Issue

Cite this: *Chem. Sci.*, 2021, **12**, 2060

All publication charges for this article have been paid for by the Royal Society of Chemistry

Received 20th October 2020
Accepted 17th December 2020

DOI: 10.1039/d0sc05785a

rsc.li/chemical-science

How many water molecules are needed to solve one?†

Alessandro Rognoni, Riccardo Conte and Michele Ceotto *

Many efforts undertaken to study the solvation process have led to general theories that may describe mean properties, but are unable to provide a detailed understanding at the molecular level. Remarkably, the basic question of how many solvent molecules are necessary to solvate one solute molecule is still open. By exploring several water aggregates of increasing complexity, in this contribution we employ semiclassical spectroscopy to determine on quantum dynamical grounds the minimal network of surrounding water molecules to make the central one display the same vibrational features of liquid water. We find out that double-acceptor double-donor tetrahedral coordination constituting the standard picture is necessary but not sufficient, and that particular care must be reserved for the quantum description of the combination band due to the coupling of the central monomer bending mode with network librations. It is actually our ability to investigate the combination band with a quantum-derived approach that allows us to answer the titular question. The minimal structure eventually responsible for proper solvation is made of a total of 21 water molecules and includes two complete solvation shells, of which the whole first one is tetrahedrally coordinated to the central molecule.

1. Introduction

The famous sorites paradox was first stated by Eubulides of Miletus in the 4th century B.C. In its original version it amounts to the question of down to which size a heap of sand can be still considered as such, when grains are removed one by one. A chemical-physical variant of the paradox can be formulated by counting how many water molecules make up the smallest water droplet, *i.e.* a supramolecular aggregate featuring the same properties as liquid water. Strictly related to this issue is the ubiquitous concept of solvation. Solvation is characterized by the nature of solute–solvent interactions, and often implies a structural reorganization of both. In the case of hydration, *i.e.* solvation performed by water, a specialized network of hydrogen bonds is built around the solute with solvent molecules arranged in shells. In practice, crucial phenomena like protein folding or reactivity in the condensed phase are strictly dependent on the mechanism of solvation. The structural organization of the solvent is also fundamental in explaining the hydrophobic force, sometimes described as the aggregation or desolvation of water repelling solutes that is thought to favor water-displacement equilibria when a ligand, such as a drug, approaches a receptor site in a hydrated protein. The principles of hydration are still debated with a constantly evolving consensus, which has moved over time from the original iceberg model to more recent and refined descriptions.[1] Therefore, it is not an overstatement to affirm that the investigation of the spatial organization and number of water molecules needed to hydrate a central target species is of utmost importance and still an open issue.[2–6]

The conclusions that can be drawn from such a study certainly depend on the polarity and structural characteristics of the solute, but perhaps the first "solute" worth studying is water itself. In spite of the many attempts, the issue has not been settled yet. The reason for this lack of success is essentially two-fold. From the experimental point of view, it is difficult to determine with sufficient precision the number of molecules constituting a water cluster of medium-large size or to identify the specific cluster arrangement under investigation. Theoretically, it is hard to include key quantum effects in a simulation involving several dozens of degrees of freedom. To investigate the solvent at the molecular level one should neither employ rigid-molecule models within coarse-grained approaches nor invoke uniform medium approximations returning average properties. Conversely, each and every solvent molecule must be described explicitly and accurately according to the laws of quantum mechanics.

Vibrational spectroscopy provides a powerful experimental and theoretical tool to get insights into the molecular structure.[7] In liquid water, the infrared (IR) spectrum is characterized by a broad band for the stretches, located between 3200 and 3550 cm^{-1}, which is strongly red shifted with respect to the corresponding lines of the isolated water molecule at 3657 and

Dipartimento di Chimica, Università degli Studi di Milano, Via Golgi 19, 20133 Milano, Italy. E-mail: michele.ceotto@unimi.it

† Electronic supplementary information (ESI) available: Theory, methodological approach, and benchmark calculations. See DOI: 10.1039/d0sc05785a

3756 wavenumbers.[8] This is determined by the unique and complex network of intermolecular hydrogen bonds which weakens the intramolecular stretches. Other relevant spectral features of liquid water include the band of hindered translations and rotations (librations) below 1000 cm^{-1}, the bending signal (at around 1650 cm^{-1}), and the combination band of librations and bendings spanning the region around 2100 cm^{-1}. The features of the liquid water IR spectrum are shown in the bottom half of Fig. 1.

We stipulate that for a water molecule to be labeled 'solvated' it must possess spectral features that resemble those of the bulk. In particular, besides the intramolecular bending and stretching signals, it is also crucial that the combination band of bending with librations matches the corresponding band of the bulk spectrum. A simple description of bulk liquid water depicts the H_2O molecules as tetrahedrally coordinated, which means that each individual acts as a double donor and double acceptor of hydrogen bonds. Reality is more complex, because liquid water is characterized by a variety of hydrogen-bond lengths and coordination numbers.[12,13] For instance, it is possible to find locally overcoordinated subunits, featuring three-acceptor two-donor configurations, which are responsible for the spectral tails at high frequency (on the acceptor side) and low frequency (on the donor side) of the stretching band.[14] Tri-, tetra-, and penta-coordinations are presumably the most common instances, and by means of Raman multivariate curve resolution spectroscopy (MCR-Raman), it has been possible to identify the contribution of tetra-coordinated molecules within the wide stretching band of liquid water.[12] Another powerful investigation tool, THz spectroscopy, covers instead the typical energy range of intermolecular interaction in condensed phases. It is able to characterize the collective motion in liquids and has permitted spectroscopic signals at 200 cm^{-1} and 80 cm^{-1} to be assigned to first and second solvation shell dynamics, respectively.[15]

The study of water clusters of increasing size provides a way to get molecular level insights into condensed phase systems like liquid water and ice.[16] Many experimental and theoretical investigations have been undertaken to describe the intermolecular interactions of these systems, going from small quasi-planar (with reference to the oxygen atoms) clusters to larger ones.[17–20] On the theoretical side, this has led to the construction of accurate potential energy surfaces (PESs),[21,22] search for geometric and energy minima in a very complicated energy landscape, and spectroscopic calculations.[23,24] For instance, the structural characteristics of water clusters beyond the transition between "all-surface" and "interior" ones have been studied. The transition takes place at $(H_2O)_{17}$ when one monomer is included in the framework built by the ensemble of the other water molecules.[25] Another remarkable and very recent study, aimed at assessing the minimum system size showing bulk-like properties, has been performed on ice I.[26] The main target of that investigation was to find the minimum dimensionality needed by a water cluster to show the hydrogen-bond pattern of ice I. Experimental studies and classical molecular dynamics simulations concerning infrared spectra and free energy estimates have been weighed in to conclude that in the range between 90 and 150 water molecules ice I is present in a mixture with amorphous clusters. In spite of such a variety of research efforts, some important aspects have not yet been sorted out and are still controversial. For instance, is tetrahedral coordination strictly necessary for a target water molecule to display the spectral properties of bulk liquid water? Is it sufficient? And, finally, what is the minimum number of water molecules required to fully solvate a single one?

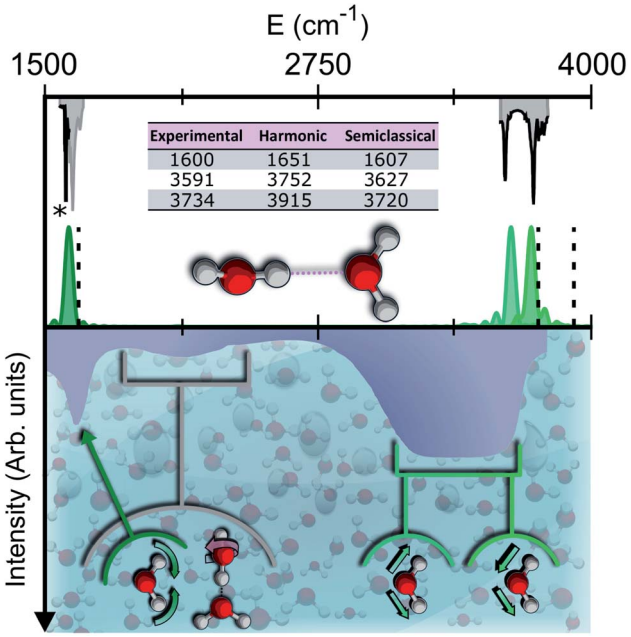

Fig. 1 Semiclassical and experimental spectra of the water dimer. Top half: comparison between the experimentally detected fundamental frequencies of vibration for the water dimer (grey)[9–11] and their theoretical semiclassical counterpart (green). The dashed vertical lines locate the harmonic estimates. The asterisk helps the eye detect the exact position of the reference experimental bending signal. Bottom half: the experimental IR spectrum of liquid water (solid contour). The normal modes involved in several signals are indicated with arrows and associated with the corresponding portions of the spectrum.

2. Results and discussion

To give a precise answer to these questions we performed a quantum investigation by means of semiclassical spectroscopy, a theoretical and computational technique suitable for dealing with high dimensional or complex systems and reproducing quantum effects starting from classical trajectories.[27–31] The upper panel of Fig. 1 demonstrates the high accuracy of SC spectroscopy in an application to the water dimer when compared with experimental results. However, it also shows that, as expected, the spectroscopic features of the water dimer (especially at high frequency) are not compatible with those of bulk water, confirming that more elaborate structures are necessary to mimic the bulk. Semiclassical methods have been applied successfully in a range going from small molecules,[32–34] including fluxional ones,[35] to medium-large systems.[36] For this work we employed the multiple coherent states divide-and-

conquer semiclassical initial value representation technique (MC-DC SCIVR),[37] which has permitted open issues concerning protonated glycine supramolecular systems to be solved[38] and has already been applied to the vibrational investigation of small water clusters.[39] The interested reader may find more theoretical information on semiclassical dynamics and spectroscopy in Section 1 of the ESI.† For our semiclassical calculations we employed the water many-body MB-pol potential energy surface.[40] We ran single-trajectory simulations about 0.7 ps long with a time step of about 0.12 fs. The initial energy of vibration was set equal to zero for the low-frequency modes (those with harmonic frequencies below the bending frequency), while the rotational and the translational motion of each monomer were eliminated at each step and the velocities were rescaled accordingly. More details to permit the reproducibility of results are provided in Section 2 of the ESI.†

Our analysis starts by studying three small water clusters: the dimer, which we have already anticipated; the trimer; the hexamer, this one in its prism configuration. The remarkable information collected from these simulations is that the frequencies of asymmetric stretches are blue shifted with respect to the experimental band of liquid water, in spite of the wide range it spans, and the bending signal is shifted from its experimental counterpart too. These spectral features demonstrate that solvation is not achieved for this set of small clusters, as confirmed by Fig. 2, which reports for the trimer and the hexamer prism the power spectra obtained for the bending and stretches of each water monomer superimposed on the IR spectrum of liquid water. Detailed frequency values can be found in Section 3 of the ESI.† We remark that the height of our peaks is not related to the experimental IR intensity (see Section 1 of the ESI).† Therefore, we have chosen to scale the intensities to ease the comparison between theory and experiments. From a structural point of view, the monomers in these small clusters are not tetrahedrally coordinated, hinting at the necessity to have an appropriate shell of coordination in order to display solvation properties, as suggested by Raman and THz spectroscopy studies. Fig. 2 also points out a key characteristic of calculated power spectra. They are able to reproduce all vibrational energy levels including those not involved in active IR or Raman transitions. For this reason our semiclassical simulations provide plenty of spectroscopic information and incorporate not only the target signals for bending and stretch fundamentals, but also combined excitations, Fermi resonances, overtones, and secondary signals related to other vibrational modes strongly coupled to the target ones. It is indeed the high density of vibrational states in association with inter-monomer interactions that shapes the wide IR bands typical of liquid water, an aspect also confirmed experimentally.[41,42]

Before moving to more complex systems, we note that there are two water oligomers that do have (in one of their several isomers) tetrahedral coordination around one of the monomers. They are the water pentamer and heptamer, for which the target stretches are well inside the corresponding IR band of liquid water (see Fig. 3). However, this does not constitute sufficient evidence of solvation. In fact, the IR spectrum of liquid water is also characterized by the presence of a band in the 1900–2300 cm^{-1} range due to combined excitations of intra-monomer bendings and inter-monomer librations, as mentioned above. This feature can be explored by exploiting the capability of semiclassical spectroscopy to recover quantum effects. Specifically, the signal of the combined excitation of the bending of the target monomer with the libration most coupled to it (according to the analysis of the Hessian matrix at the equilibrium configuration) has been simulated showing that it is located outside the corresponding band in liquid water. This proves that even the presence of a 4-monomer coordination shell is not sufficient to achieve solvation, and an investigation at the quantum level able to reproduce combination bands is fundamental to point out this aspect. Furthermore, for tetrahedrally coordinated water molecules we can employ the MCR-Raman spectrum presented in ref. 12 to narrow the stretching band of liquid water. In Fig. 3, the MCR-Raman spectrum has been highlighted.

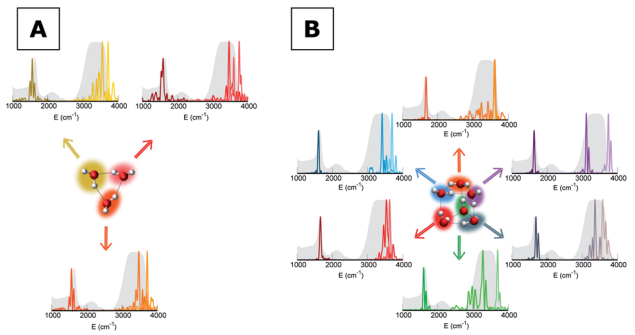

Fig. 2 Power spectra for bending and stretches of individual monomers of small water clusters. (A) Trimer and (B) hexamer prism. The colored haloes link each monomer to the appropriate power spectrum. Color nuances are darker for bendings and lighter for symmetric and asymmetric stretches. The IR spectrum of liquid water is reported as shaded gray areas. The intensities of power spectra have been scaled to match the maximum of the corresponding experimental IR band.

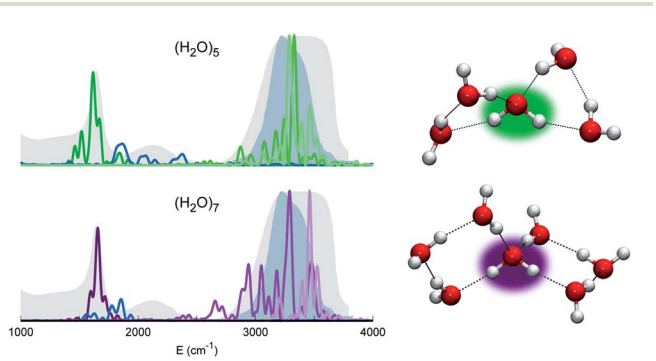

Fig. 3 Power spectra of the tetrahedrally coordinated monomer in different water clusters. Top left column: pentamer; bottom left column: heptamer. The combined excitation of the bending with the most coupled libration mode is also reported in dark blue. The liquid water IR spectrum is shown as shaded gray areas, and the MCR-Raman band (from ref. 12) for the stretches of tetrahedrally coordinated monomers in liquid water (light blue) is also presented.

We note that, while the pentamer with its unperturbed tetrahedral coordination has both stretches well within the band, the asymmetric stretch for the heptamer is displaced toward the border of it. This is interpreted as the effect due to two additional monomers not directly coordinated to the central molecule, a first clear indication that tetrahedral coordination is not sufficient, and that a more extended network is required to reproduce the solvation features.

Therefore, our quest for the minimal solvation structure proceeds by investigating more sizable systems for which a double shell of coordination around a central, target monomer is present. This is the case, for instance, of $(H_2O)_{19}$. The spectral features of the central monomer of this aggregate are shown in Fig. 4. Even if the results are closing in toward the expected spectroscopic characteristics of a solvated molecule, some inconsistencies are still present. The bending signal is shifted from the corresponding band in liquid water, and the stretches, even if located at still reasonable frequencies, are quite blue shifted with respect to the tetrahedral coordination band. We reckon that another, more complex structure needs to be studied and move to $(H_2O)_{21}$. In this case, the spectroscopic features of the bending and stretches of the target monomer are exactly where they are expected to be for a solvated water molecule. The final check is given by the combination peak, which is located at 1950 cm^{-1}, *i.e.* still within the range of the IR experimental combination band. For these reasons our guess is that $(H_2O)_{21}$ represents the smallest water aggregate in which one monomer is solvated in the same way as molecules in the liquid.

To confirm this hypothesis we also analyzed a bigger structure, *i.e.* $(H_2O)_{23}$. In this case, even the combination signal moves to the center of the liquid water band, confirming that a solvation structure has indeed been reached. This shift is due to the higher frequency of the libration mode most coupled to the target bending (about 240 cm^{-1} at the harmonic level) in the case of $(H_2O)_{23}$ with respect to $(H_2O)_{21}$. In the $(H_2O)_{23}$ cluster, similarly to the heptamer but in a less prominent way, the asymmetric signal moves toward the edge of the tetrahedral coordination band revealing that, even if solvation is maintained, the two additional monomers have slightly influenced the coordination and solvation network. Detailed results can be found in Section 3 of the ESI.†

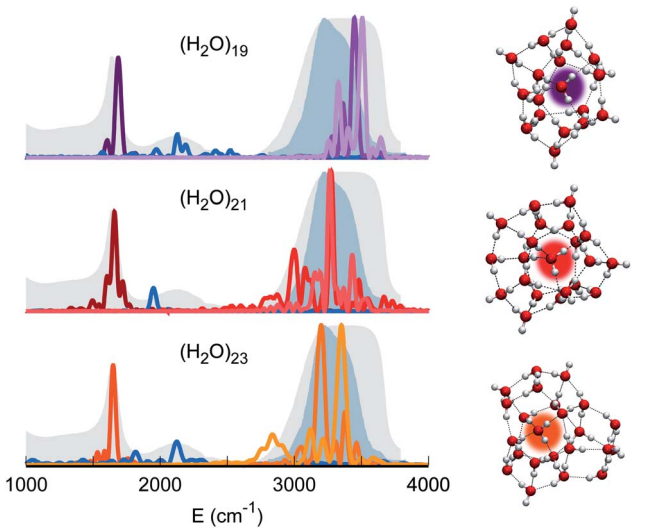

Fig. 4 Power spectra of the target monomer for larger clusters. The peaks corresponding to bendings, stretches, and combined bending-libration bands of $(H_2O)_{19}$ (top), $(H_2O)_{21}$ (middle), and $(H_2O)_{23}$ (bottom) are reported.

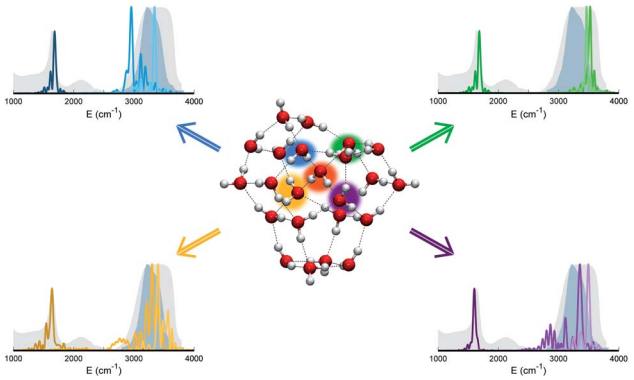

Fig. 5 Power spectra of bending and stretch signals for the four monomers that are hydrogen bonded to the central monomer in $(H_2O)_{23}$. Different monomers and the corresponding power spectra are indicated with different colors (blue, green, violet, and yellow). The central monomer is highlighted in orange. Despite the tetrahedral coordination of these monomers, none of them matches the liquid water experimental spectra.

The persistent influence of outer additional monomers triggered our interest in having a closer look at the structural properties of $(H_2O)_{23}$. In particular, Fig. 5 focuses on the four monomers constituting the first coordination shell for the central one. Each of these four water molecules is itself tetrahedrally coordinated, but several spectral features do not match the liquid water ones. This is further confirmation that tetrahedral coordination alone does not warrant solvation, and that it is necessary to account for the overall network of hydrogen interactions which provides a complex and cooperative way for solvation in water.

3. Conclusions

Even though the bands characterizing the IR spectrum of liquid water are necessarily broad, a comparison with the results of accurate quantum spectroscopic simulations is able to discriminate the effective solvation properties of a central molecule embedded in clusters of increasing size. Small water clusters like the dimer, trimer, and hexamer are spectroscopically incompatible with solvation and their structure obviously lacks an appropriate coordination shell, which is found instead in the pentamer and heptamer that display tetracoordination at the central molecule. However, even in these latter oligomers the target spectral features do not match those of liquid water with reference to the combination band of bending and librations. Eventually, the size of the water aggregate had to be raised to 21 monomers in order to find the first example of a structure

providing a proper solvation of its central molecule. This finding was confirmed by the study of a 23-monomer cluster. The bottom line is that tetrahedral coordination is a necessary but not sufficient condition; the minimal solvation structure, the primary aim of our quest, is found to consist of a central water molecule surrounded by at least 20 water monomers organized in a double coordination shell. Substantial cooperative effects through the extended bonding manifold are at work in determining the spectral properties of water solvation.

Conflicts of interest

There are no conflicts to declare.

Acknowledgements

The authors thank Professor A. Gavezzotti for his careful reading of the manuscript. The authors acknowledge financial support from the European Research Council [Grant Agreement No. (647107) – SEMICOMPLEX – ERC-2014-CoG] under the European Union's Horizon 2020 research and innovation programme and from the Italian Ministry of Education, University, and Research (MIUR) (FARE programme Grant No. R16KN7XBRB-project QURE).

Notes and references

1 H. S. Frank and M. W. Evans, *J. Chem. Phys.*, 1945, **13**, 507–532.
2 O. Mishima and H. Stanley, *Nature*, 1998, **396**, 329–335.
3 J. Errington and P. Debenedetti, *Nature*, 2001, **409**, 318–321.
4 D. Marx, *Science*, 2004, **303**, 634–636.
5 C. A. Angell, *Science*, 2008, **319**, 582–587.
6 J. A. Fournier, C. J. Johnson, C. T. Wolke, G. H. Weddle, A. B. Wolk and M. A. Johnson, *Science*, 2014, **344**, 1009–1012.
7 C. Aieta, M. Micciarelli, G. Bertaina and M. Ceotto, *Nat. Commun.*, 2020, **11**, 1–9.
8 A. G. Csaszar, E. Matyus, T. Szidarovszky, L. Lodi, N. F. Zobov, S. V. Shirin, O. L. Polyansky and J. Tennyson, *J. Quant. Spectrosc. Radiat. Transfer*, 2010, **111**, 1043–1064.
9 R. H. Page, J. G. Frey, Y. Lee and Y.-R. Shen, *Chem. Phys. Lett.*, 1984, **106**, 373–376.
10 G. Ayers and A. Pullin, *Spectrochim. Acta, Part A*, 1976, **32**, 1629–1639.
11 Y. Bouteiller and J. Perchard, *Chem. Phys.*, 2004, **305**, 1–12.
12 D. Ben-Amotz, *J. Am. Chem. Soc.*, 2019, **141**, 10569–10580.
13 J. A. Fournier, C. T. Wolke, C. J. Johnson, M. A. Johnson, N. Heine, S. Gewinner, W. Schöllkopf, T. K. Esser, M. R. Fagiani, H. Knorke and K. R. Asmis, *Proc. Natl. Acad. Sci.*, 2014, **111**, 18132–18137.
14 T. Morawietz, A. S. Urbina, P. K. Wise, X. Wu, W. Lu, D. Ben-Amotz and T. E. Markland, *J. Phys. Chem. Lett.*, 2019, **10**, 6067–6073.
15 M. Heyden, J. Sun, S. Funkner, G. Mathias, H. Forbert, M. Havenith and D. Marx, *Proc. Natl. Acad. Sci. U. S. A.*, 2010, **107**, 12068–12073.
16 N. Yang, C. H. Duong, P. J. Kelleher, A. B. McCoy and M. A. Johnson, *Science*, 2019, **364**, 275–278.
17 Y. Wang and J. M. Bowman, *J. Chem. Phys.*, 2011, **134**, 154510.
18 R. Schwan, M. Kaufmann, D. Leicht, G. Schwaab and M. Havenith, *Phys. Chem. Chem. Phys.*, 2016, **18**, 24063–24069.
19 J. O. Richardson, C. Pérez, S. Lobsiger, A. A. Reid, B. Temelso, G. C. Shields, Z. Kisiel, D. J. Wales, B. H. Pate and S. C. Althorpe, *Science*, 2016, **351**, 1310–1313.
20 A. Rakshit, P. Bandyopadhyay, J. P. Heindel and S. S. Xantheas, *J. Chem. Phys.*, 2019, **151**, 214307.
21 Y. Wang, B. C. Shepler, B. J. Braams and J. M. Bowman, *J. Chem. Phys.*, 2009, **131**, 054511.
22 Y. Wang and J. M. Bowman, *Phys. Chem. Chem. Phys.*, 2016, **18**, 24057–24062.
23 D. J. Wales, *J. Am. Chem. Soc.*, 1993, **115**, 11180–11190.
24 R. J. Saykally and D. J. Wales, *Science*, 2012, **336**, 814–815.
25 C. C. Pradzynski, C. W. Dierking, F. Zurheide, R. M. Forck, U. Buck, T. Zeuch and S. S. Xantheas, *Phys. Chem. Chem. Phys.*, 2014, **16**, 26691–26696.
26 D. R. Moberg, D. Becker, C. W. Dierking, F. Zurheide, B. Bandow, U. Buck, A. Hudait, V. Molinero, F. Paesani and T. Zeuch, *Proc. Natl. Acad. Sci. U. S. A.*, 2019, **116**, 24413–24419.
27 W. H. Miller, *Adv. Chem. Phys.*, 1974, **25**, 69–177.
28 E. J. Heller, *Acc. Chem. Res.*, 1981, **14**, 368–375.
29 M. F. Herman and E. Kluk, *Chem. Phys.*, 1984, **91**, 27–34.
30 A. L. Kaledin and W. H. Miller, *J. Chem. Phys.*, 2003, **118**, 7174–7182.
31 W. H. Miller, *Proc. Natl. Acad. Sci. U. S. A.*, 2005, **102**, 6660–6664.
32 A. L. Kaledin and W. H. Miller, *J. Chem. Phys.*, 2003, **119**, 3078–3084.
33 R. Conte, A. Aspuru-Guzik and M. Ceotto, *J. Phys. Chem. Lett.*, 2013, **4**, 3407–3412.
34 F. Gabas, R. Conte and M. Ceotto, *J. Chem. Theory Comput.*, 2017, **13**, 2378.
35 G. Bertaina, G. Di Liberto and M. Ceotto, *J. Chem. Phys.*, 2019, **151**, 114307.
36 F. Gabas, R. Conte and M. Ceotto, *J. Chem. Theory Comput.*, 2020, **16**, 3476–3485.
37 M. Ceotto, G. Di Liberto and R. Conte, *Phys. Rev. Lett.*, 2017, **119**, 010401.
38 F. Gabas, G. Di Liberto, R. Conte and M. Ceotto, *Chem. Sci.*, 2018, **9**, 7894–7901.
39 G. Di Liberto, R. Conte and M. Ceotto, *J. Chem. Phys.*, 2018, **148**, 104302.
40 G. R. Medders, V. Babin and F. Paesani, *J. Chem. Theory Comput.*, 2014, **10**, 2906–2910.
41 B. Wang, W. Jiang, Y. Gao, Z. Zhang, C. Sun, F. Liu and Z. Wang, *RSC Adv.*, 2017, **7**, 11680–11683.
42 N. Yang, C. H. Duong, P. J. Kelleher and M. A. Johnson, *Nat. Chem.*, 2020, **12**, 159–164.

Electronic Supplementary Material (ESI) for Chemical Science.

Supplementary Information for

How many water molecules are needed to solvate one?

Alessandro Rognoni, Riccardo Conte, and Michele Ceotto*

E-mail: michele.ceotto@unimi.it

This PDF file includes:

Contents

1 Theory

1.1 Semiclassical spectroscopy: A powerful quantum investigation technique

In molecular spectroscopy quantum aspects like zero-point energies, tunneling splittings, overtones, and combined excitations are of great importance. Purely quantum investigations are doable for small systems, but they become quickly computationally unaffordable as the complexity of the system under study increases. In spite of their intrinsic limitations and inaccuracies, *ad hoc* scaled harmonic approaches and classical investigations are usually undertaken in absence of a quantum treatment[1,2]. Semiclassical (SC) spectroscopy is a recently developed technique able to combine the advantages of classical and quantum spectroscopy into a novel and powerful investigation tool[3]. It has already been adopted to study the vibrational features of large molecules like fullerene[4], and biomolecules like glycine, nucleobases, and dipeptide derivatives[5–7]. Furthermore, SC spectroscopy has permitted to solve open issues related to supra-molecular systems. This is the case of some peculiar vibrational features of the glycine dimer and H_2-tagged protonated glycine, which have been successfully explained by means of SC spectroscopy[8]. All these results and other recent investigations provide a solid background for the investigations presented in the main body of this manuscript[6,9–19].

The foundation of semiclassical spectroscopy lies in the possibility to get the eigenvalues of the vibrational Hamiltonian starting from the Fourier transform of the survival amplitude

$$I(E) \propto \int dt\, e^{iEt/\hbar} \langle \Psi_0 | \Psi(t) \rangle, \tag{1}$$

where $|\Psi_0\rangle$ is an arbitrary state and $I(E)$ is the density of vibrational states. If one describes this arbitrary state as a linear combination of the Hamiltonian eigenstates $|E_j\rangle$, i.e. $|\Psi_0\rangle =$

$\sum_j c_j|E_j\rangle$, then Eq. (1) can be recast as

$$I(E) = \sum_j |c_j|^2 \delta(E - E_j), \tag{2}$$

which clearly demonstrates that peaks in the plot of $I(E)$ are centered at the vibrational eigenvalues.

Eq. (1) requires to evolve the initial state $|\Psi_0\rangle$ for a time t. In SC dynamics this is done by means of the SC propagator, whose most popular version is known as the Herman-Kluk propagator[20]. The reference state evolved in time using the Herman-Kluk propagator takes the form:

$$|\Psi(t)\rangle = \frac{1}{(2\pi\hbar)^{N_{vib}}} \int\int d\mathbf{p}_0 d\mathbf{q}_0 \, C_t(\mathbf{p}_0, \mathbf{q}_0) \, e^{iS_t(\mathbf{p}_0,\mathbf{q}_0)/\hbar} \, \langle \mathbf{p}_0, \mathbf{q}_0 | \Psi_0 \rangle | \mathbf{p}_t, \mathbf{q}_t \rangle. \tag{3}$$

Semiclassical propagation according to Eq. (3) requires to run full (N_{vib})-dimensional classical trajectories for a total time t, usually of the order of one picosecond, starting from momenta and coordinates $(\mathbf{p}_0, \mathbf{q}_0)$. For this reason the initial value representation (IVR) denomination is often used to describe the method[21]. The instantaneous classical action $S_t(\mathbf{p}_0, \mathbf{q}_0)$ and the complex-valued prefactor $C_t(\mathbf{p}_0, \mathbf{q}_0)$ are fingerprints of the original derivation of the SCIVR theory as stationary phase approximation to Feynman's path integral representation of the quantum propagator[22]. Finally, the $|\mathbf{p}_0, \mathbf{q}_0\rangle$ and $|\mathbf{p}_t, \mathbf{q}_t\rangle$ states are the initial and time-evolved basis set coherent states. It is this sophisticated mathematical machinery which permits the quantitative description of quantum effects starting from classical trajectories.

For application of SC dynamics to the evaluation of Eq. (1), Kaledin and Miller introduced their time-averaged formulation of the Herman-Kluk propagator and worked out the following SC expression for the spectral density

$$I(E) \propto \int\int d\mathbf{p}_0 d\mathbf{q}_0 \left| \int_0^T dt\, e^{i[S_t(\mathbf{p}_0,\mathbf{q}_0)+\phi_t(\mathbf{p}_0,\mathbf{q}_0)+Et]/\hbar} \langle \mathbf{p}_t,\mathbf{q}_t|\Psi_0\rangle \right|^2 , \quad (4)$$

where the total evolution time is indicated by T and only the phase of the prefactor $\phi_t(\mathbf{p}_0, \mathbf{q}_0)$ is employed. As anticipated, a plot of $I(E)$ versus E, i.e. the power spectrum of the vibrational Hamiltonian, allows one to identify the eigenvalues as the energies at which the several spectral signals are centered. The corresponding frequencies of vibration are readily obtained by difference with respect to the ZPE value. Our power spectra provide a quantum comparison to experimental IR and Raman spectra regarding the vibrational frequencies, a feature which is at the heart of the investigations described in the main body of the manuscript.

Eq. (4) requires a phase space integration which is computationally unaffordable as the system dimensionality increases beyond a few degrees of freedom. In this case it is necessary to rely on a SC technique able to provide accurate vibrational frequencies from a single or few trajectories. The multiple coherent states semiclassical approach (MC SCIVR) makes this possible[9]. It is based on the fact that quantum eigenvalues can be estimated exactly by a single-trajectory SC simulation, provided that the classical trajectory is run at that exact energy[23]. Clearly the exact energy is not known *a priori*, but the MC-SCIVR technique provides anyway a very accurate approximation to it. The approach adopts the same mathematical formalism of Eq. (4) but relies on the choice of tailored reference states able to enhance the spectral signal associated to the energy at which the simulation is performed. Furthermore, the MC SCIVR has opened the possibility to adopt direct *ab initio* molecular dynamics for SC spectroscopy with application to medium-large systems for which accurate analytical potential energy surfaces are not available.

Notwithstanding, application of SC spectroscopy to large systems has been hampered by the difficulty to get sensible spectroscopic signals when the quantum overlap in Eq. (4) is

not sizeable due to its multi-dimensional product nature. To overcome this major issue, very recently, the divide-and-conquer SC method (DC SCIVR) has been introduced[4,15]. The working equation of DC SCIVR is similar to Eq. (4) but based on the projection of the several dynamical quantities onto lower dimensional subspaces appropriately chosen to accommodate strongly coupled vibrational modes

$$\tilde{I}(E) \propto \int\int d\tilde{\mathbf{p}}_0 d\tilde{\mathbf{q}}_0 \left| \int_0^T dt\, e^{i[\tilde{S}_t(\tilde{\mathbf{p}}_0,\tilde{\mathbf{q}}_0)+\tilde{\phi}_t(\tilde{\mathbf{p}}_0,\tilde{\mathbf{q}}_0)+Et]/\hbar} \langle \tilde{\mathbf{p}}_t, \tilde{\mathbf{q}}_t | \tilde{\Psi}_0 \rangle \right|^2 . \tag{5}$$

The total power spectrum is eventually reconstructed as a convolution of the lower dimensional spectra, and the tilde symbol (~) has been added to those quantities that have been projected onto a M-dimensional subspace. All the quantities appearing in Eq. (5) can be straightforwardly projected, with the exception of the action. This happens because the potential V of the systems under investigation is not separable (it cannot be written down exactly as a sum of terms coming from different subspaces). To project the action we adopted the following equation:

$$\tilde{S}_t(\tilde{\boldsymbol{p}}_0, \tilde{\boldsymbol{q}}_0) = \int_0^t dt' \left[\frac{1}{2} \tilde{\boldsymbol{p}}_{t'}{}^T \tilde{\boldsymbol{p}}_{t'} - \left(V(\tilde{\boldsymbol{q}}_{t'}, \boldsymbol{q}_{t'}^{(N_{vib}-M)}) - V(\tilde{\boldsymbol{q}}_{eq}, \boldsymbol{q}_{t'}^{(N_{vib}-M)}) \right) \right], \tag{6}$$

which is exact for separable systems and approximates the projected action for non-separable ones. The multiple coherent and divide-and-conquer techniques can be interfaced leading to single-trajectory simulations for subspaces of reduced dimensionality. The technique is called multiple coherent states divide-and-conquer semiclassical initial value representation (MC-DC SCIVR), which is indeed the kind of approach adopted for the investigations presented in the main body of the manuscript. The key observation that allows one to reduce the number of trajectories is that most of the contribution to the spectrum comes from the trajectories having an energy as close as possible to the true but unknown quantum mechanical eigenvalues. On

this basis, in the multiple coherent framework proper initial conditions and tailored reference states are employed to decrease the number of trajectories down to one per simulation.

For any target state α (like the ground state or excited states), the reference state $|\tilde{\Psi}_0\rangle$ can be chosen as a combination of coherent states

$$|\tilde{\Psi}_0\rangle_\alpha = \prod_{k=1}^{M} |\tilde{p}_k^{eq}, \tilde{q}_k^{eq}\rangle + \varepsilon_{k,\alpha}| - \tilde{p}_k^{eq}, \tilde{q}_k^{eq}\rangle. \tag{7}$$

In the previous equation, $\tilde{\mathbf{q}}^{eq}$ are the equilibrium positions and $\tilde{\mathbf{p}}^{eq}$ the harmonically approximated mass-scaled momenta

$$\tilde{p}_k^{eq} = \sqrt{\hbar\omega_k(2n_k+1)}, \tag{8}$$

where ω_k is the harmonic frequency of the k-th mode and n_k its vibrational quantum number. In Eq. (7), $\varepsilon_{k,\alpha}$ is the k-th component of an M-dimensional array of integers appropriately chosen to enhance the spectral signal associated to the specific state α. For instance, a collection of $\epsilon_{k,\alpha} = +1$ values allows one to get the ZPE signal. As another example, if only the k'-th element of the array is equal to -1 (with all other array elements equal +1), then the spectral features corresponding to α states that in harmonic approximation have an odd number of quanta in the k'-th degree of freedom are emphasized. The procedure is rigorous in the case of uncoupled harmonic oscillators, and only approximated but still very helpful in the general case, in which less intense signals due to states strongly coupled to the α one may also be present.

2 Methodological approach

2.1 Assigning normal modes to specific water monomers

In water clusters, the normal modes are strongly delocalized over different water molecules. So, the assignment of a vibrational mode to a specific monomer must be done carefully. For assigning the normal modes to specific water molecules, we relied on the time-averaged root-mean-square displacement (TA RMSD). Specifically, we considered one vibrational mode at a time, leaving the others at their equilibrium values. Along the trajectory of the select mode, we summed up the deviation from the equilibrium positions of all the water molecules that compose the cluster. At the end of the trajectory, we assigned the vibrational normal mode to the water molecule with the highest TA RMSD. The underlying principle is that if a normal mode primarily contributes to the motion of a specific monomer, then it will be assigned to that water molecule. This approach corresponds to the usual chemical interpretation of the assignment procedure. Table 1 reports the values of TA RMSD of the central water molecule of $(H_2O)_{21}$ obtained for all the bendings and stretches. The three normal modes assigned to the central water molecule are q_{132} (bending), q_{149}, and q_{153} (stretches). Fig. 1 shows the behavior of TA RMSD with respect to the central water molecule of the three select normal modes.

The distinction between symmetric and asymmetric stretches is a more complex task because the same normal mode can act with a symmetric character on a water molecule but with an asymmetric character on another one. To distinguish the symmetric stretches from the asymmetric ones, we adopted an approach based on a reward function. For each stretching mode and at each time-step of the trajectory, a reward of +1 is assigned to a monomer if the two OH distances change in the same direction, *i.e.* if the stretch is symmetric. In the same fashion, a -1 reward is assigned if the OH distances change in opposite directions, the key feature of asymmetric stretch. It is noteworthy that we always obtained full (either positive or negative) rewards

for all the stretches of the clusters we studied. This means that even though the same normal mode can have different behavior when acting on different monomers, its pure symmetric or asymmetric character is preserved along the trajectory. In fig. 2 we showed the two types of reward plot we obtained for all the stretches studied in this work. Depending on the normal mode under consideration and on the water molecule it is attributed to, the reward is always positive (symmetric stretch) or always negative (asymmetric stretch). As anticipated earlier and in the main text, for all the simulations we employed a single classical trajectory, using the MC-DC SCIVR method developed by our group.

Table 1: **Values of TA RMSD with respect to the motion of the central water molecule obtained for all the bendings and stretches of the $(H_2O)_{21}$ cluster.** The normal modes "q" are labeled according to their harmonic frequencies. It is possible to observe that the three normal modes 132, 149, and 153 (one bending and two stretches) can be unambiguously assigned to the central water molecule of the cluster.

q	TA RMSD/au		q	TA RMSD/au	
132	1.24	10^{-1}	**156**	8.22	10^{-3}
149	9.13	10^{-2}	**134**	8.17	⋮
153	9.11	⋮	**141**	7.05	
137	8.66		**167**	6.63	
154	6.99		**129**	6.16	
130	6.37		**144**	4.75	
122	5.82		**145**	4.68	
131	4.08		**171**	4.09	
150	3.61		**125**	4.03	
168	2.90		**161**	3.40	
124	2.48		**163**	2.99	
151	2.44		**147**	2.12	
158	2.35		**165**	2.01	
157	2.25		**142**	1.89	
138	2.21		**175**	1.79	
126	2.19		**143**	1.52	
160	2.15		**172**	1.22	
139	2.09		**146**	1.19	
133	2.01		**123**	1.16	
159	1.92		**170**	1.05	
166	1.88		**179**	9.17	10^{-4}
155	1.86		**164**	8.23	⋮
152	1.73		**181**	7.68	
136	1.39		**178**	3.96	
128	1.38		**174**	3.91	
121	1.33		**173**	3.31	
162	1.19		**176**	3.12	
135	1.07		**177**	2.81	
169	9.75	10^{-3}	**182**	2.31	
127	9.75	⋮	**183**	1.99	
140	9.00		**180**	1.93	
148	8.24				

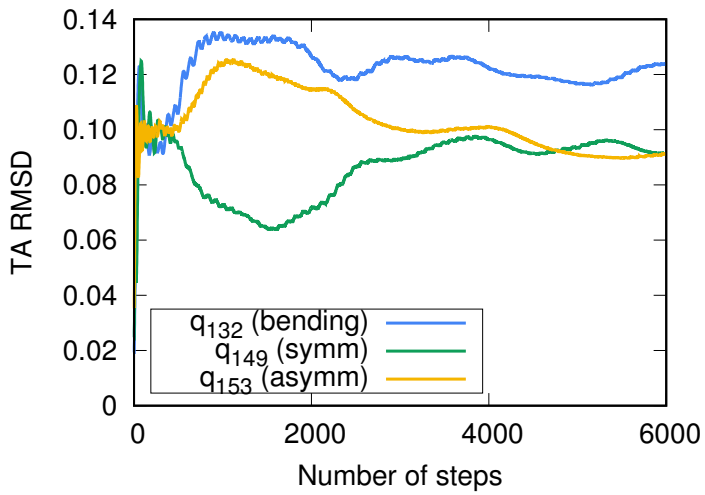

Figure 1: **Behavior of TA RMSD for the normal modes assigned to the central monomer of the $(H_2O)_{21}$ cluster. q_{132}: bending; q_{149}: symmetric stretch; q_{153}: asymmetric stretch.**

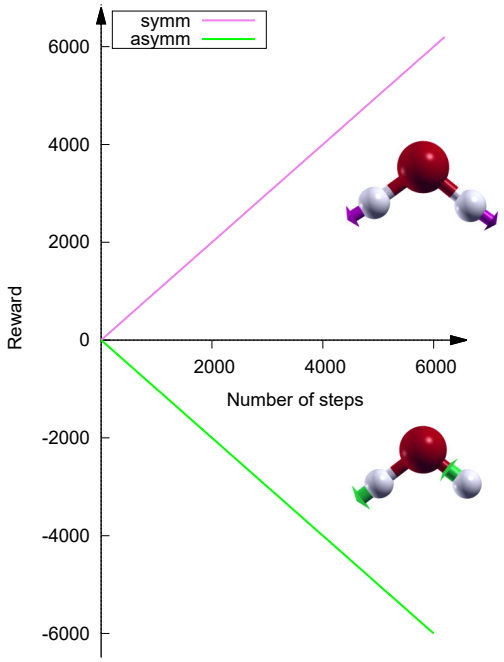

Figure 2: **Rewards obtained for all the stretches analyzed in this work.** Violet: reward assigned to symmetric stretches. Green: same but referred to asymmetric stretches. Our simulations are made of 6000 steps, so it is clear that we always obtain full (positive or negative) rewards.

2.2 Combination band calculation

Once the bending associated to central monomer has been assigned, it is possible to calculate the band associated to the combined excitation of the bending with all the low-frequency librational modes. This band would span a very large portion of the spectrum because, for a general $(H_2O)_n$ cluster, there are $6(n-1)$ low-frequency vibrational normal modes, and hence $6(n-1)$ combination signals. To obtain results comparable between the several water aggregates investigated, we chose to focus on the libration that exhibits the highest coupling with the bending of the central water molecule.

The challenge now is how to recognize this special librational mode. First of all, a ZPE trajectory is run (a 0.7 ps-long trajectory with a timestep of 0.12 fs), without removing the angular momentum of the water molecules from the trajectory. In fact, the low-frequency modes are usually characterized by hindered rotations or translations, which could not be accurately described using the same approach employed for the intramolecular mode simulations. Along this trajectory, we apply the Hessian method developed by our group to identify the librational mode showing the highest coupling with the bending. In practice, the off-diagonal elements of the Hessian matrix, which correspond to the second derivative of the potential with respect to the bending and to the different librations, are calculated and their absolute values are summed up. In this way, we obtained time-averaged Hessian matrix elements, which are a direct measure of the coupling between normal modes. Specifically, the off-diagonal elements of the Hessian are equal to zero in the case of completely uncoupled oscillators. So, the magnitude of the mixed derivative of the potential with respect to two normal modes is a measure of their coupling. Therefore, the libration experiencing the highest coupling with the bending of the central monomer will be the one with the highest off-diagonal element of the time-averaged Hessian matrix. Fig. 3 shows the chosen libration for the $(H_2O)_{21}$ cluster. In fig. 4 we reported the behavior of the time-averaged off-diagonal elements of the Hessian matrix for different librational

modes. Once the target libration has been determined, it is possible to calculate the combination signal through a proper choice of the wavepacket. In this case, both the ϵ coefficients of Eq. (7) associated to the target bending and libration are set equal to -1, while leaving all the others equal to 0.

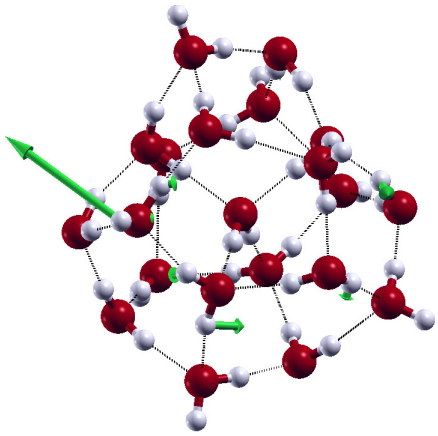

Figure 3: **Selected libration for the $(H_2O)_{21}$ cluster**. This normal mode is labeled q_{53} in Fig. 4.

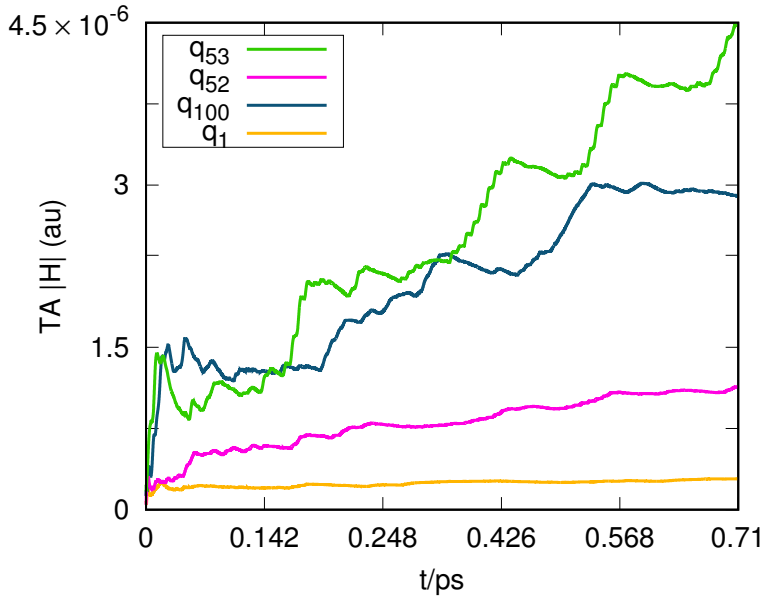

Figure 4: **Time-averaged absolute values of the Hessian matrix for the bending of the central monomer of $(H_2O)_{21}$.** The time-averaged matrix elements are compared for different librational motions: q_{53} is the select libration (reported in Fig. 3), q_{52} is a libration with similar harmonic frequency, q_1 is a libration with lower harmonic frequency, and q_{100} is characterized by a higher harmonic frequency.

3 Benchmark calculations

3.1 Vibrational frequencies of small-dimensional water clusters

Here we report the frequency values obtained with the MC-DC-SCIVR approach and discussed in the main text. The results are benchmarked against experiments and MultiMode (MM) or Local Monomer Model (LMM) calculations. Both the MM and the LMM simulations were carried out on a different potential energy surface (the WHBB one)[24]. Nonetheless, these values provide an accurate qualitative benchmark to confirm the accuracy of the MC-DC-SCIVR method. The vibrational spectrum of the water dimer is depicted in Fig. 5 and the corresponding frequencies are reported in Table 2. The vibrational frequencies of the water trimer and of the

water hexamer prism (Fig. 2 in the main text) are listed in Table 3 and in Table 4, respectively.

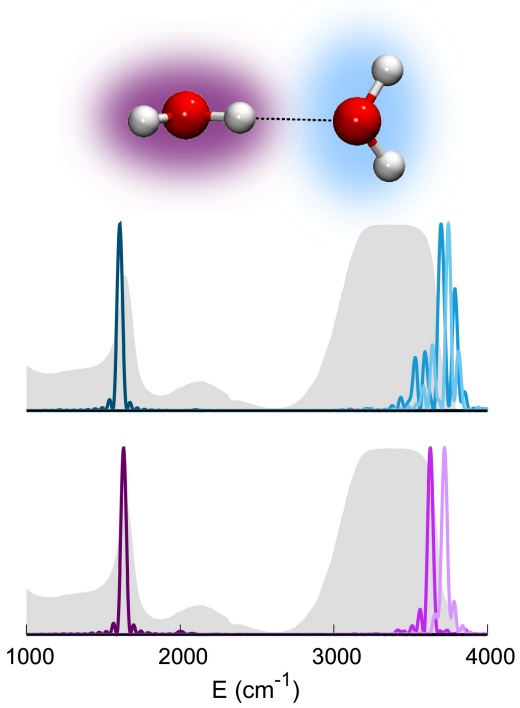

Figure 5: **Vibrational spectrum of the water dimer.** Peak colors are chosen in agreement with the water monomer they belong to. The liquid water infrared spectrum is reported as shaded gray areas.

Table 2: **Frequencies of the water dimer (cm^{-1}).** Column "q" reports the normal modes ordered according to their harmonic frequencies (Harm); column "MM" shows the MultiMode estimates; column "MC-DC SCIVR" reports the semiclassical frequencies obtained in the present work; under column "Exp" we have reported the experimental frequencies[25]. Mean absolute errors with respect to experiments (MAE exp) and MM calculations (MAE MM) are shown. The spectrum can be found in fig. 1 of the main text.

q	Exp	MM	MC-DC SCIVR	Harm
7	1600	1588	1607	1651
8	1617	1603	1632	1665
9	3591	3573	3627	3752
10	3661	3627	3698	3832
11	3734	3709	3720	3915
12	3750	3713	3745	3935
MAE exp	-	23	19	133
MAE MM	-	-	36	156

Table 3: **Frequencies of the water trimer (cm^{-1}). Labels are chosen in agreement with Table 2.**

q	MM	MC-DC SCIVR	Harm
13	1597	1562	1656
14	1600	1591	1661
15	1623	1561	1685
16	3486	3465	3636
17	3504	3550	3685
18	3514	3475	3694
19	3709	3753	3906
20	3716	3714	3915
21	3720	3714	3916
MAE MM	-	29	143

Table 4: **Frequencies of the water hexamer prism (cm^{-1}). Labels are chosen in agreement with Table 2. Under column "LMM" we have reported the Local Monomer Model estimates.**

q	LMM	MC-DC SCIVR	Harm
31	1606	1605	1652
32	1612	1600	1671
33	1620	1630	1680
34	1633	1659	1690
35	1654	1669	1711
36	1677	1682	1729
37	3092	3114	3307
38	3256	3283	3513
39	3372	3361	3603
40	3442	3412	3627
41	3482	3534	3729
42	3521	3622	3747
43	3579	3578	3789
44	3588	3627	3805
45	3630	3609	3818
46	3697	3739	3908
47	3706	3701	3910
48	3728	3694	3911
MAE LMM	-	25	161

3.2 Vibrational frequencies of tetrahedrally coordinated water molecules

In this section we report the frequencies associated to bendings, stretches and combination bands of water molecules with tetrahedral coordination. Table 5 reports the frequencies of the central water monomers of $(H_2O)_5$ and $(H_2O)_7$. Table 6 reports the vibrational frequencies of the central water molecule in larger water clusters. Specifically, Table 7 shows the vibrational frequencies of the monomers that make up the first solvation shell of the central water molecule of $(H_2O)_{23}$ (depicted in Fig. 6).

In Tables 5, 6, and 7, the vibrational frequencies of the target water molecules are high-

lighted if they are compatible with the experimental frequencies of liquid water. We remark that this comparison can be made only from a qualitative point of view. In fact, we can only rely on broad infrared signals to confirm the solvation of a target water molecule. Raman-MCR experiments somewhat help to narrow the stretching band in the case of tetrahedrally coordinated water molecules, but the signal still remains quite broad. At present, we can only give a qualitative description of a solvated water molecule. Any well-defined energy window that discriminates a solvated water molecule from a non-solvated one would not be neither accurate nor very helpful. More specifically, a plethora of stretching signals are compatible with a solvated water molecule within the experimental band, given the infinity number of geometries that it can assume.

Table 5: **Frequencies associated to the central monomers of small water clusters (cm^{-1}).** The corresponding MC-DC-SCIVR power spectra are reported in Fig. 3 of the main text. The MC-DC-SCIVR frequencies are reported under columns "SC", while the harmonic frequencies are listed under columns "Harm". Frequencies of bendings and combination bands that are comparable with the ones of the liquid water infrared spectrum as well as signals associated to symmetric and asymmetric stretches comparable with the MCR-Raman spectrum are highlighted.

	$(H_2O)_5$		$(H_2O)_7$	
	SC	**Harm**	**SC**	**Harm**
bending	**1616**	1662	**1656**	1680
combination band	1863	1902	1854	1909
symmetric stretch	**3329**	3600	**3290**	3469
asymmetric stretch	**3288**	3722	3461	3583

Table 6: **Frequencies associated to the central monomers of larger water clusters (cm^{-1}).** The corresponding MC-DC-SCIVR power spectra are reported in Fig. 4 of the main text. Labels are chosen in agreement with Table 5. Frequencies of bendings and combination bands that are comparable with the ones of the liquid water infrared spectrum as well as signals associated to symmetric and asymmetric stretches comparable with the MCR-Raman spectrum are highlighted.

	$(H_2O)_{19}$		$(H_2O)_{21}$		$(H_2O)_{23}$	
	SC	**Harm**	**SC**	**Harm**	**SC**	**Harm**
bending	1687	1696	**1659**	1697	**1649**	1709
combination band	**2127**	2313	**1950**	1980	**2124**	2233
symmetric stretch	3448	3607	**3276**	3462	**3200**	3425
asymmetric stretch	3506	3583	**3253**	3538	**3351**	3465

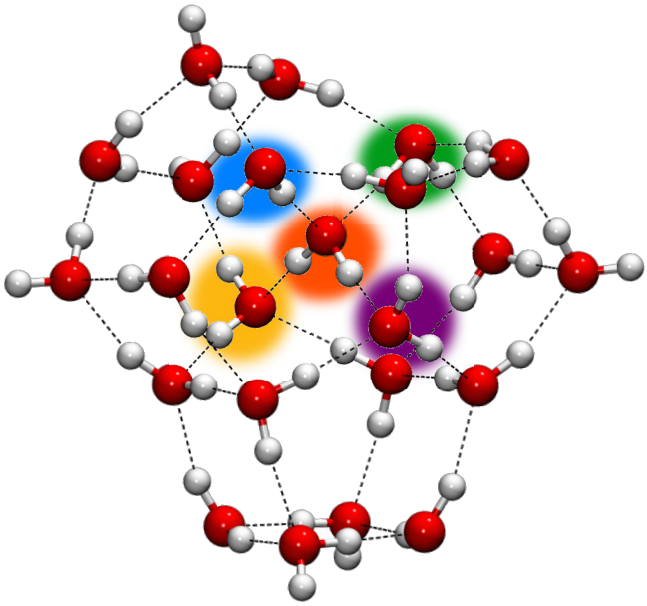

Figure 6: **Magnified view of the $(H_2O)_{23}$ cluster.** The monomers composing the first solvation shell of the central water molecule are highlighted with different colors (yellow, blue, green, and purple). The central water molecule is colored in orange.

Table 7: **MC-DC SCIVR frequencies associated to the monomers constituting the first coordination shell of the $(H_2O)_{23}$ cluster (cm^{-1}).** The colors of the labels are chosen to match the corresponding monomers in the previous figure. Frequencies of bendings and combination bands that match the IR spectrum of liquid water as well as signals associated to symmetric and asymmetric stretches matching the MCR-Raman spectrum are highlighted.

$(H_2O)_{23}$	Mon1	Mon2	Mon3	Mon4
bending	1684	**1640**	1602	1684
symmetric stretch	2961	**3303**	**3353**	3525
asymmetric stretch	**3343**	3402	3494	3465

References

(1) Scott, A. P.; Radom, L. Harmonic vibrational frequencies: an evaluation of Hartree-Fock, Møller- Plesset, quadratic configuration interaction, density functional theory, and semiempirical scale factors. *J. Phys. Chem.* **1996**, *100*, 16502–16513.

(2) Galimberti, D. R.; Milani, A.; Tommasini, M.; Castiglioni, C.; Gaigeot, M.-P. Combining static and dynamical approaches for infrared spectra calculations of gas phase molecules and clusters. *Journal of chemical theory and computation* **2017**, *13*, 3802–3813.

(3) Miller, W. H. Quantum dynamics of complex molecular systems. *Proc. Natl. Acad. Sci. USA* **2005**, *102*, 6660–6664.

(4) Ceotto, M.; Di Liberto, G.; Conte, R. Semiclassical "divide-and-conquer" method for spectroscopic calculations of high dimensional molecular systems. *Phys. Rev. Lett.* **2017**, *119*, 010401.

(5) Gabas, F.; Conte, R.; Ceotto, M. On-the-fly ab initio semiclassical calculation of glycine vibrational spectrum. *J. Chem. Theory Comput.* **2017**, *13*, 2378.

(6) Gabas, F.; Di Liberto, G.; Ceotto, M. Vibrational investigation of nucleobases by means of divide and conquer semiclassical dynamics. *J. Chem. Phys.* **2019**, *150*, 224107.

(7) Conte, R.; Gabas, F.; Botti, G.; Zhuang, Y.; Ceotto, M. Semiclassical vibrational spectroscopy with Hessian databases. *J. Chem. Phys.* **2019**, *150*, 244118.

(8) Gabas, F.; Di Liberto, G.; Conte, R.; Ceotto, M. Protonated glycine supramolecular systems: the need for quantum dynamics. *Chem. Sci.* **2018**, *9*, 7894–7901.

(9) Ceotto, M.; Atahan, S.; Tantardini, G. F.; Aspuru-Guzik, A. Multiple coherent states for first-principles semiclassical initial value representation molecular dynamics. *J. Chem. Phys.* **2009**, *130*, 234113.

(10) Ceotto, M.; Atahan, S.; Shim, S.; Tantardini, G. F.; Aspuru-Guzik, A. First-principles semiclassical initial value representation molecular dynamics. *Phys. Chem. Chem. Phys.* **2009**, *11*, 3861–3867.

(11) Ceotto, M.; Tantardini, G. F.; Aspuru-Guzik, A. Fighting the curse of dimensionality in first-principles semiclassical calculations: Non-local reference states for large number of dimensions. *J. Chem. Phys.* **2011**, *135*, 214108.

(12) Conte, R.; Aspuru-Guzik, A.; Ceotto, M. Reproducing deep tunneling splittings, resonances, and quantum frequencies in vibrational spectra from a handful of direct ab initio semiclassical trajectories. *J. Phys. Chem. Lett.* **2013**, *4*, 3407–3412.

(13) Di Liberto, G.; Ceotto, M. The importance of the pre-exponential factor in semiclassical molecular dynamics. *J. Chem. Phys.* **2016**, *145*, 144107.

(14) Micciarelli, M.; Conte, R.; Suarez, J.; Ceotto, M. Anharmonic vibrational eigenfunctions

and infrared spectra from semiclassical molecular dynamics. *J. Chem. Phys.* **2018**, *149*, 064115.

(15) Di Liberto, G.; Conte, R.; Ceotto, M. "Divide and conquer" semiclassical molecular dynamics: A practical method for spectroscopic calculations of high dimensional molecular systems. *J. Chem. Phys.* **2018**, *148*, 014307.

(16) Buchholz, M.; Grossmann, F.; Ceotto, M. Simplified approach to the mixed time-averaging semiclassical initial value representation for the calculation of dense vibrational spectra. *J. Chem. Phys.* **2018**, *148*, 114107.

(17) Bertaina, G.; Di Liberto, G.; Ceotto, M. Reduced rovibrational coupling Cartesian dynamics for semiclassical calculations: Application to the spectrum of the Zundel cation. *J. Chem. Phys.* **2019**, *151*, 114307.

(18) Conte, R.; Parma, L.; Aieta, C.; Rognoni, A.; Ceotto, M. Improved semiclassical dynamics through adiabatic switching trajectory sampling. *J. Chem. Phys.* **2019**, *151*, 214107.

(19) Micciarelli, M.; Gabas, F.; Conte, R.; Ceotto, M. An Effective Semiclassical Approach to IR Spectroscopy. *J. Chem. Phys.* **2019**, *150*, 184113.

(20) Herman, M. F.; Kluk, E. A semiclassical justification for the use of non-spreading wavepackets in dynamics calculations. *Chem. Phys.* **1984**, *91*, 27–34.

(21) Miller, W. H.; George, T. F. Semiclassical theory of electronic transitions in low energy atomic and molecular collisions involving several nuclear degrees of freedom. *J. Chem. Phys.* **1972**, *56*, 5637–5652.

(22) Feynman, R. P.; Hibbs, A. R. *Quantum mechanics and path integrals*; McGraw-Hill, 1965.

(23) De Leon, N.; Heller, E. J. Semiclassical quantization and extraction of eigenfunctions using arbitrary trajectories. *J. Chem. Phys.* **1983**, *78*, 4005–4017.

(24) Wang, Y.; Bowman, J. M. Ab initio potential and dipole moment surfaces for water. II. Local-monomer calculations of the infrared spectra of water clusters. *J. Chem. Phys.* **2011**, *134*, 154510.

(25) Bouteiller, Y.; Perchard, J. The vibrational spectrum of $(H_2O)_2$: Comparison between anharmonic ab initio calculations and neon matrix infrared data between 9000 and 90 cm^{-1}. *Chem. Phys.* **2004**, *305*, 1–12.